Summer 8-31-2013

Solar eclipse observation on may 21, 2012 from JVLA

Shaheda Begum Shaik
New Jersey Institute of Technology

Copyright Warning & Restrictions

The copyright law of the United States (Title 17, United States Code) governs the making of photocopies or other reproductions of copyrighted material.

Under certain conditions specified in the law, libraries and archives are authorized to furnish a photocopy or other reproduction. One of these specified conditions is that the photocopy or reproduction is not to be "used for any purpose other than private study, scholarship, or research." If a, user makes a request for, or later uses, a photocopy or reproduction for purposes in excess of "fair use" that user may be liable for copyright infringement,

This institution reserves the right to refuse to accept a copying order if, in its judgment, fulfillment of the order would involve violation of copyright law.

Please Note: The author retains the copyright while the New Jersey Institute of Technology reserves the right to distribute this thesis or dissertation

Printing note: If you do not wish to print this page, then select "Pages from: first page # to: last page #" on the print dialog screen

ABSTRACT

SOLAR ECLIPSE OBSERVATION ON MAY 21, 2012 FROM JVLA

by
Shaheda Begum Shaik

The annular solar eclipse occurred on May 21, 2012 is studied using the radio data from the Jansky Very Large Array (JVLA), Sorrocco, Mexico. The eclipse is observed in the solar minimum activity period of solar cycle 24. The centimeter wavelength observation of the Sun's surface during the solar eclipse helps in determining the spatially well resolved features not obtained by the man made advanced technology. Even though, the activity on the Sun is observed to be low in the period of eclipse, the study provides a good opportunity to understand the quiet Sun features in the regions occulted by the Moon.

Rather than observing the Sun during the eclipse as a whole map of the entire field of view, differential technique is used to map strips of the field of view covered and obscured by the Moon's limb. This study is an attempt to understand the emission mechanism in the active region structures and the quiet Sun regions by realizing the change in the intensity levels of the observation than the intensity itself. During this work, it is discovered at least one anomaly in the data, called delay clunking, which reduces the frequency resolution to 125 MHz in 16 frequencies over the 2-4 GHz band. At the selected frequency of 2.56 GHz, the peak brightness temperature corresponding to both the active regions observed show 90% increase over the quiet Sun region value.

Even though the bright source like feature in the synthesis map does not show much variations in its size, it shows intensity enhancement at the peak occultation than the regions (quiet Sun) where the Moon is away from the active region. The correlation of the radio maps with the Solar Dynamo Observatory (SDO) show a good response to further study the JVLA data with a recheck in the calibration and with a higher frequency resolution.

SOLAR ECLIPSE OBSERVATION ON MAY 21, 2012 FROM JVLA

by
Shaheda Begum Shaik

A Thesis
Submitted to the Faculty of
New Jersey Institute of Technology
and Rutgers, The State University of New Jersey – Newark
in Partial Fulfillment of the Requirements for the Degree of
Master of Science in Applied Physics

Federated Department of Physics

August 2013

APPROVAL PAGE

SOLAR ECLIPSE OBSERVATION ON MAY 21, 2012 FROM JVLA

Shaheda Begum Shaik

Dr. Dale E. Gary, Thesis Advisor — Date
Distinguished Professor of Physics, NJIT

Dr. Haimin Wang, Committee Member — Date
Distinguished Professor of Physics, NJIT

Dr. Gregory Fleishman, Committee Member — Date
Research Professor, CSTR, NJIT

BIOGRAPHICAL SKETCH

Author: Shaheda Begum Shaik

Degree: Masters Degree

Date: August 2013

Undergraduate and Graduate Education:

- Master of Science in Applied Physics,
  New Jersey Institute of Technology, Newark, NJ, 2013

- Master of Science in Electronics,
  Bharathidasan University, Trichy, India, 2007

- Bachelor of Science in Maths, Physics, Electronics (Triple major),
  Sri Venkateswara University, Tirupati, India, 2005

Major: Applied Physics

Presentations and Publications:

M. Lahkar, P. K. Manoharan, K. Mahalakshmi, K. Prabhu, G. Agalya, S. Shaheda Begum and P. Revathi, "The interplanetary consequences of a large CME" in Astrophysics and Space Science Proceedings, 'Magnetic coupling between the interior and the atmosphere of the Sun', Springer-Verlag Berlin Heidelberg, 2010.

A. R. Rao, J. P. Malkar, M. K. Hingar, V. K. Agrawal, S. K. Chakrabarti, A. Nandi, D. Debnath, T. B. Kotoch, T. R. Chidambaram, P. Vinod, S. Sreekumar, Y. D. Kotov, A. S. Buslov, V. N. Yurov, V. G. Tyshkevich, A. I.Arkhangelskij, R. A. Zyatkov, S. Shaheda Begum and P. K. Manoharan, "RT-2 detection of quasi-periodic pulsations in the 2009 July 5 solar hard x-ray flare", The Astrophysical Journal, Volume 714, Issue 2, pp. 1142-1148, 2010.

S. Sreekumar, P. Vinod, Essy Samuel, J. P. Malkar, A. R. Rao, M. K. Hingar, V. P. Madhav, D. Debnath, T. C. Kotoch, Anuj Nandi, S. Shaheda Begum and Sandip K. Chakrabarti, "Instruments and their test and evaluation of RT-2 payloads aboard CORONAS-PHOTON V: Onboard software, Data Structure, Telemetry and Telecommand", Experimental Astronomy, Volume 29, Issue 1-2, pp 109-133, February 2011.

ACKNOWLEDGMENT

I express my gratitude to my thesis advisor, Dr. Dale E. Gary for his advice, support and guidance throughout my project for helping me in optimizing in this work.

I thank my committee members Dr. Haimin Wang and Dr. Gregory Fleishman for readily accepting to be the members of the thesis committee.

My special thanks to Dr. Samuel Tun whose suggestions and ideas were helpful during the analysis.

Finally, I would like to thank my family members and friends for their moral support, without which it would have been impossible to achieve this.

TABLE OF CONTENTS

Chapter	Page
1 INTRODUCTION	1
1.1 Solar Eclipse Observation on May 21, 2012	1
1.2 Solar Eclipse	2
1.3 Interferometry	7
1.4 Importance of Solar Eclipse Radio Observation	9
2 BACKGROUND OF THIS STUDY	11
2.1 Solar Magnetic Phenomena	11
2.1.1 Quiet Sun	12
2.1.2 Active Sun	14
2.2 Radio Observations	15
2.2.1 Free-free Emission	17
2.2.2 Gyroresonance Radio Emission	17
2.2.3 Coronal Magnetic Field Measurement	17
3 DATA AND OBSERVATION	20
3.1 JVLA Interferometer	20

TABLE OF CONTENTS
(Continued)

Chapter **Page**

3.2 Observational Setup..... 22

3.3 Data Structure and Tools Used..... 25

4 DATA ANALYSIS – MAPPING..... 27

4.1 Calibration..... 27

4.2 Light Curves and Spectra..... 28

4.3 Mapping..... 32

4.4 CLEAN Technique..... 33

4.5 Correlation with the Space Observation..... 34

5 CONCLUSION..... 37

REFERENCES..... 38

LIST OF FIGURES

Figure		Page
1.1	A comparative geometry of the Moon's shadow on the Earth's surface in the solar eclipse for the nearest and the farthest Moon-Earth distances.....	4
1.2	The points of contact in a total and an annular solar eclipse.....	6
2.1	Total solar eclipse showing solar corona.....	13
2.2	A comparison of the radiation from the Sun at different wavelengths.....	13
2.3	Characteristics radio frequencies for the solar atmosphere.....	16
2.4	Radio emission spectra at two lines of sight in a model active region.....	18
3.1	VLA array in Y shape configuration.....	21
3.2	The path of annularity over the globe.....	22
3.3	The uneclipsed Sun as seen in HMI magnetogram and the eclipse geometry.....	23
3.4	Close-ups of and AR 11482 and AR 11484.....	24
4.1	Peak brightness distribution in amplitude, phase variations and HMI map of AR1.....	29
4.2	Time series of amplitude and phase variations of AR2.....	30

LIST OF FIGURES
(Continued)

Figure **Page**

4.3 Dynamic spectrum of AR1 as a function of frequency (2 to 4 GHz) with time averaged over 10 s..... 31

4.4 Uncleaned map with the Sun's (blue) and Moon's (green) limbs marked for AR2 at 2.56 GHz..... 32

4.5 Cleaned maps merged over time give the orientation of the lunar limb for AR1 and AR2 at 2.56 GHz..... 34

4.6 The JVLA eclipse clean map of AR1 at 3.3 GHz overlaid on HMI magnetogram 35

4.7 The JVLA clean map overlay and contour with the HMI magnetogram at the peak of the eclipse on AR2..... 36

CHAPTER 1

INTRODUCTION

1.1 Solar Eclipse Observation on May 21, 2012

An annular solar eclipse was observed on May 21, 2012 with the National Radio Astronomy Observatory's Jansky Very Large Array (JVLA), near Socorro, New Mexico at a microwave frequency range of 2-4 GHz. The interferometric complex visibility data from 23 antennas is analyzed to image the occulted regions on the Sun's surface by the Moon during the eclipse. The activity level of the Sun is quiet with few less-complex bipolar active regions. There are no intense flare events observed on the day and during the eclipse.

The quiet Sun observations in the frequency range of 2 to 4 GHz (or 15 to 7.5 centimeter wavelength) range are helpful to reveal the spatially resolved small scale structures of the quiet Sun surface and the low level activities occurring in the active regions.

The microwave interferometric studies of solar eclipses have helped over years to achieve the high spatial resolution of active regions with free-free emission and gyro-resonance emissions (e.g., Gary and Hurford, 1987). Studies using interferometric data from seven antennas (21 baselines) were used to obtain synthesis maps of 2.5″x12.7″ resolution, which showed a small number of compact sources in the quiet Sun regions with mean angular size and peak brightness temperature in the range 9″- 25″ and (6-8) x 10^4 K (Marsh, Hurford and Zirin, 1980). At relatively short wavelengths (<6cm), the most intense emission is usually located above the sunspots where high magnetic fields

allow the detection of thermal gyroresonance radiation at coronal heights (Alissandrakis, Kundu, and Lantos, 1980; Lang and Willson, 1982). In the current study, with a large number of baselines (253) of 23 antennas it is aimed to determine the source structures in the microwave radiation of the active regions from the images obtained from the interferometric technique in comparison with the high resolution SDO (Solar Dynamic Observatory) images and to determine the characteristics of the observed radiation at free free and gyroresonance emission. The main advance is potentially the high frequency resolution of the VLA after its recent expansion, which provides thousands of frequencies over the 2-4 GHz range, although these observations were taken in the "Shared Risk" period when the VLA is not guaranteed to perform to its ultimate capabilities. During the work on this thesis, it is discovered at least one anomaly in the data, so-called "delay clunking," which causes the measured phases to deviate from their optimum values for IF (intermediate frequency) channels away from the band centre. Due to this limitation, it is chosen to integrate over each IF band of 125 MHz, so that the frequency resolution is only 125 MHz, providing 16 frequencies over the 2-4 GHz band.

1.2 Solar Eclipse

Any astronomical object moving in its orbit may obscured/occulted by another body passing between it and the observer, leading to an eclipse. In our solar system, solar and lunar eclipses are predominantly observed, with shadows falling on the Earth and the Moon by the light from the Sun. These eclipses occur when the Sun, Earth and Moon are aligned in a straight line casting shadows. In a lunar eclipse, the Earth is between the Sun and Moon, where the Moon passes through the shadow cast by the Earth. In a solar

eclipse, the Moon passes between the Earth and Sun, where the Moon occults the Sun as viewed from the Earth and casts its shadow on the Earth's surface. As the purpose of this study is to observe a solar eclipse, in particular the geometry of solar the eclipse is discussed here.

In the solar eclipse, the Sun can be obscured either fully or partially, depending on the distance of the Earth from the Moon (i.e., relative distance of the Moon from Earth ranging from its apogee to perigee) and the observing point in the region of shadow on the Earth's surface. The Moon's orbit is elliptical and is tilted by 5 degrees to the Earth's ecliptic plane. With this geometry, the Sun, Earth and Moon line up at least twice a year leading to an eclipse of the Sun that can be observed from the region of shadow of the Moon.

During a solar eclipse, the Moon's shadow is observed to have three parts on the Earth's surface because of the elliptical orbit of the Moon. The umbra, the region of observation with dark inner shadow in which the Moon fully obscures the Sun, is shown in the Figure 1.1 The antumbra, the region beyond the end of the umbra, is farther from the Moon, making it too small to cover the Sun's surface completely. The penumbra is the region of faint outer shadow in which the Moon partially covers the Sun.

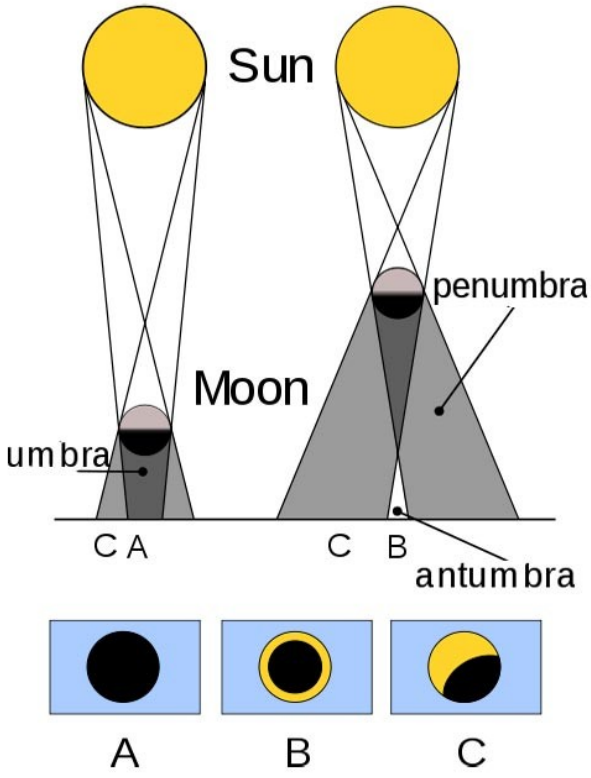

Figure 1.1 A comparative geometry of the Moon's shadow on the Earth's surface in the solar eclipse for the nearest and the farthest Moon-Earth distances.

Source: http://en.wikipedia.org/wiki/File:Solar_eclipse_types.svg and http://flatrock.org.nz

Observing the Sun from any point on the Earth's surface with these three parts of shadows classify the solar eclipse in four general classes.

1. Total solar eclipse
2. Partial solar eclipse
3. Annular solar eclipse
4. Hybrid solar eclipse

A total solar eclipse occurs when the Moon completely obscures the Sun as it is observed from the region on the Earth's surface where umbra of the Moon's shadow falls (Figure 1.1, case A). The moon on its orbit has to be closer to the Earth (near perigee) for

a total eclipse to occur. As the angular diameter of the Moon (30 arc minute) at this stage is about the same as that of the Sun, the former covers the solar disk i.e., the photosphere, allowing the outer corona to be visible. Thus, a total eclipse serves as a rare opportunity to study the faint corona.

A partial solar eclipse (as shown in Figure 1.1, case C) is seen in penumbra, which occurs when the Moon partially obscures the Sun, as the name reflects. In this case, the Sun, Earth and Moon are not aligned exactly, but the eclipse can be observed from the larger area of the Moon's shadow, the penumbra. Depending on the observer's location in the area of penumbra the extent of the partial obscuring of the Sun varies.

An annular or ring eclipse passes across the centre of the solar disk when the Moon is in a distant part (near apogee) of its orbit from the Earth. The apparent size of the Moon is smaller than that of the Sun making the Sun's surface to appear as a bright ring or annulus around the Moon as shown in the Figure 1.1, case B. As the moon is farther from the Earth, the umbral shadow of the Moon never reaches Earth, but rather the ring occurs for observers within the antumbral shadow.

Basically, the difference in occurrence of total and annular eclipse is due to the Moon's elliptical orbit, and the varying distance between the Moon and Earth, leading to the different apparent sizes of the Moon. To a lesser extent, the elliptical orbit of the Earth around the Sun also leads to variations in the apparent size of the Sun. The width of the path track of the eclipse on the Earth's surface depends on the relative apparent sizes of the Moon and Sun.

As shown in the Figure 1.2, different phases are observed during an eclipse. These phases over time provide different stages of covering and revealing Sun's surface leading

to understand the structures and phenomena on the Sun and the Moon.

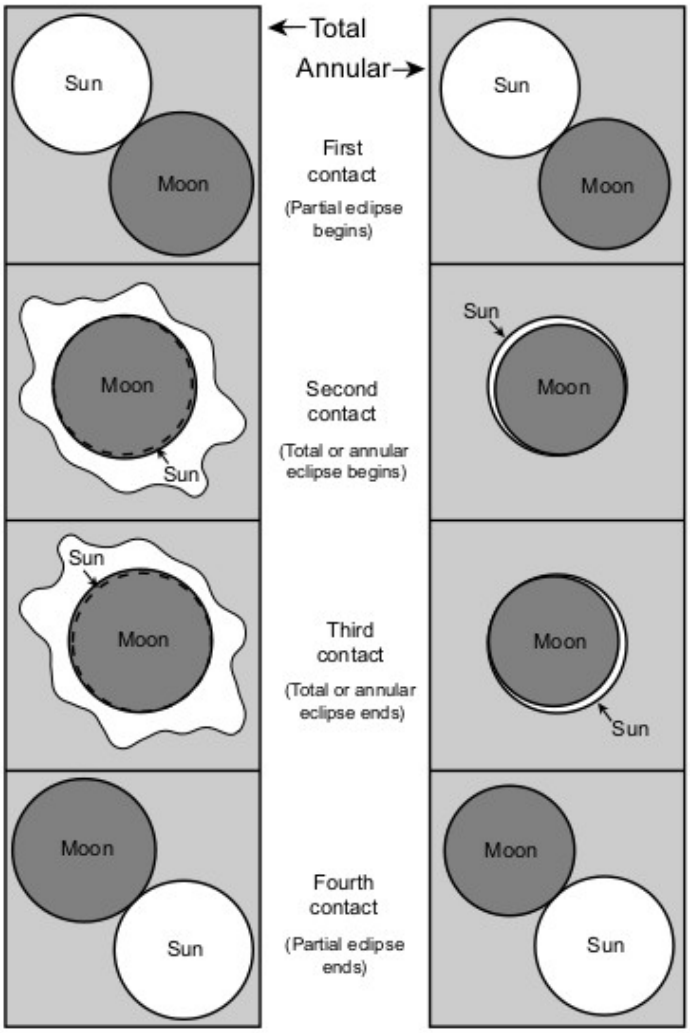

Figure 1.2 The points of contact in a total (left) and an annular solar eclipse (right). A partial eclipse has only first and fourth point of contacts.

Source: Totality Eclipses of the Sun , Mark Littmann , Fred Espenak & Ken Willcox

Along the path of eclipse on the Earth's surface a hybrid eclipse is viewed as a total and an annular eclipse. Because of the Earth's curvature, the Moon's umbra falls on some locations along the path while the antumbra falls on the more distant locations.

1.3 Interferometry

Interferometry is the important technique used in astronomy to study the electromagnetic waves when superimposed. A single antenna or a telescope is used to collect electromagnetic radiation from the astronomical objects, with the angular resolution depending on the size (diameter) of the antenna used and the wavelength observed. An interferometer is an array of antennas used to combine signals giving a resolution more than a single antenna. In the case of an interferometer, resolution is given by the maximum distance between the antennas in the array. The spread of the antennas gives the same angular resolution as an antenna of the size of the entire spread.

Interferometry is used to diagnose the original state of the waves before the superposition by determining the phase difference between waves of the same frequency. The waves in phase superimpose constructively, giving peak amplitude and the waves that are out of phase superimpose destructively, giving a smaller amplitude. An interferometer uses the technique of aperture synthesis with a cluster of antennas in a pattern, with longer baselines allowing arcsecond or sub-arcsecond resolution observations. A baseline is the separation between two antennas in the interferometer, whose number in an array is given by $n(n-1)/2$, where n is the total number of antennas.

Each antenna in the interferometer measures the amplitude and the phase of the incoming signal from the far away object observed. Combining all the signals from each antenna, the output from the interferometer is the Fourier transformed information of the brightness distribution of the observed object.

The complex visibility is that Fourier transformed output which is given by

$$V(u,v) = \int I(l,m)\, exp[-i2\pi(ul + vm)]\ \ dl\ \ dm \qquad (1.1)$$

where u,v are the projected baseline lengths measured in the units of wavelength, $I(l,m)$ is the sky brightness distribution with l,m as the sky components relative to a reference position in the E-W and N-S directions. The sampled visibility function is the output provided by the interferometric array. The dirty image is obtained by performing the inverse Fourier transform given as,

$$I_D(l,m) = \int S(u,v)V(u,v)exp[i2\pi(ul + vm)]\ \ du\ dv \qquad (1.2)$$

where S is the so-called sampling function provided by the positions of the antennas in the array.

As the dirty map is obtained from the sampled visibility function, it does not give the complete picture of the sky brightness distribution observed, but is affected by gaps in the coverage (missing u,v spacings). These gaps are filled to have more complete information by using an image reconstruction technique like CLEAN, MEM, etc. The method of processing the interferometer data is further discussed in the forthcoming chapters.

There are many interferometer sites available all over the world to attempt the desired benefits expected from interferometry. The Very Large Array (VLA), and the Very Long Baseline Array (VLBA) are some radio astronomical interferometers currently used to observe astronomical bodies in their range of observing frequency of radio radiation.

The VLA consists of 27 independent antennas each with a diameter of 25 meters spread as an array along linear three arms in a 'Y' shape, with an observing frequency range of 75 MHz to 40 GHz, although only portions of this range can be observed at any one time. The longest baseline is 36 km (acts as an antenna with 36 km diameter) reaching a good angular resolution of 0.05 arcsec at 7 mm of observing wavelength. VLBI technique uses many antennas that are widely spaced around the world giving a very large baseline extent over the size of a continent or even greater. VLBI achieves milli-arcsec resolution to accurately measure small sources and their positions, although it has not proven useful for studying the relatively nearby sun.

1.4. Importance of Solar Eclipse Radio Observations

There are a vast number of advanced techniques to observe the solar corona and the magnetic features in that region of the solar atmosphere. The angular resolution plays a main limitation in the observations. As discussed in Section 1.3, the size of the antenna or an interferometer required to be suitable for a given observing frequency to probe the solar atmosphere and the magnetic structures in it with arcsec resolution. The Sun presents a difficult challenge for high-resolution imaging, because it is a very large, complex, and constantly changing source. Not only high resolution (provided by long baselines) is needed, but simultaneously very good image quality (requiring many, many baselines). At present, no radio telescope exists that can image the complex full disk of the Sun all at once with high resolution.

A solar eclipse provides a means to limit the extent and complexity of the region of the Sun to be imaged. It potentially can provide extremely high angular resolution

images of a portion of the Sun's surface due to the trajectory of the Moon over it. The Earth-Moon distance plays the important factor in determining the angular resolution, but not the size of the antenna used. Even a small portable antenna of a few meters can be used to observe corona, with the Earth-Moon distance of ~0.38 million km, giving an angular resolution of ~12 arcsec at 100 MHz (http://www.iiap.res.in/solareclipse/eclipse_annular).

The moving Moon's limb gives snapshots of the region over which it is passing by taking a difference in the two successive visibility measurements as discussed earlier. Each difference contains the brightness distribution contributed by the features in the region of the Sun's surface covered or uncovered by the Moon during the integration time. This is the differential technique for mapping, which is used in the current study. Providing a very high resolution while at the same time limiting the region of the Sun to be imaged is the main benefit in making a solar eclipse observation.

CHAPTER 2

BACKGROUND OF THIS STUDY

The objective of this study is to analyze the structures observed on the surface of the Sun during the eclipse, when the Moon passes over the Sun as viewed from the path of annularity. In this chapter, a background of some characteristics of the Sun's surface and phenomena, relevant to the current study is discussed.

2.1 Solar Magnetic Phenomena

The Sun has different layers with different depths and temperatures. The layer of photosphere is where the granulation takes place and where in the limb bright patches of faculae are seen. The photosphere is the layer where one can see dark regions of higher magnetic field; the magnetic field breaks through the surface from below to produce dark regions called sunspots. These sunspots last from a few hours to several months depending on the activity of the solar cycle they are in. This photosphere is the visible layer with temperature ranging from 4500 to 6000 K.

Above this layer lies the chromosphere extending to 2,000 km of height with a density less than the photosphere. The corona, the outermost layer of the Sun, lies beyond the chromosphere with very low density compared to the lower layers of the Sun, but with very high temperature in the millions of kelvin. The magnetic phenomena, which are slowly or rapidly varying are observed in the chromosphere and extending into the corona.

According to the activity level of the solar cycle, the Sun's outer surface consists of complex magnetic structures in active regions, prominences, coronal holes, streamers or quiet regions. Active regions are area of concentrated magnetic flux above and surrounding sunspots. Active regions have a temperature ranging from $< 10^4$ K to $> 10^6$ K, which makes them to visible at wavelengths from infrared through X-rays. This magnetic field breaking through the surface (photosphere and chromosphere) can form giant arches of hot plasma (Mason & Tripathi, 2008).

2.1.1 Quiet Sun

The chromosphere has some interesting phenomena such as spicules, prominences, H alpha network, active regions, and solar flares. During an eclipse, the chromosphere appears as a red or pink ring surrounding the Sun. At the chromospheric boundary or limb, jets and spicules are observed distinctly when observed during a total solar eclipse. The phenomena of spicules, active regions, plages, filaments, and flares can be seen on the chromospheric disk.

The phenomena of the eclipse and the coincidence of the nearly same angular diameter of the Sun and the Moon helped to show the existence of the solar corona around the Sun, including streamers and prominences. A total solar eclipse, in addition to blocking the solar disk, reduces the sky brightness by around 4 orders of magnitude to make it possible to view the less dense corona.

The solar corona is a region of complex magnetic loops that are been generated within the Sun and emerge through the surface. The corona consists of helmet streamers, plumes extending from near the surface to the far interplanetary medium.

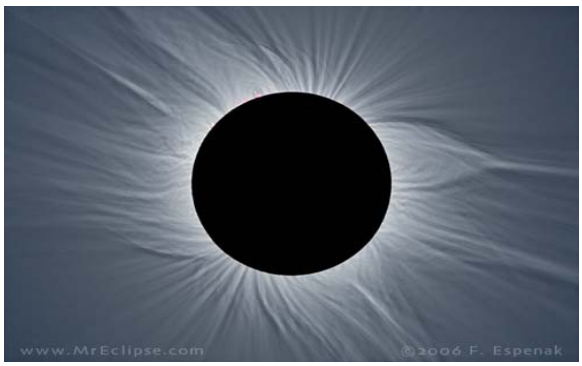

Figure 2.1 Total solar eclipse showing solar corona with streamers extending out in the space. A small portion of the pink chromosphere is also seen on the top left of the disk.

Source: http://www.mreclipse.com

The solar magnetic field plays an important role in defining the corona for its structure. The corona is optically thin in visible wavelengths, therefore coronal features on the solar disk are not seen in visible light. The on disk features of corona are seen in short wavelengths of X-rays and UV, which are not produced in the cooler photosphere.

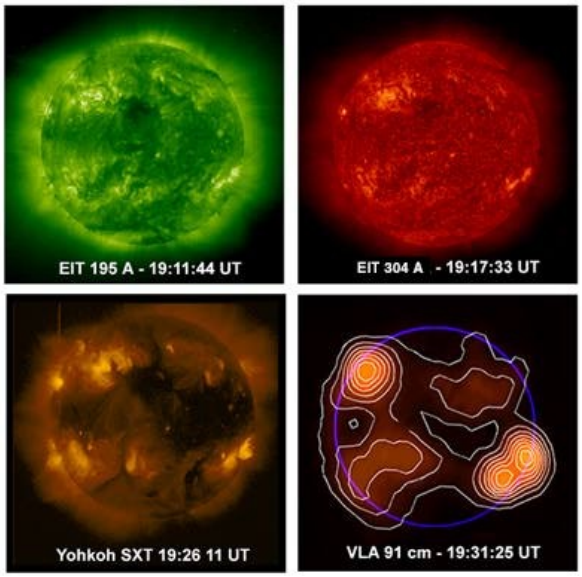

Figure 2.2 A comparison of the radiation from the Sun at different wavelengths. The VLA centimeter wavelength images are compared with the YOHKOH X-ray and EIT extreme ultraviolet images for the observation on 2 July, 2005.

Source: Willson and Groff, 2008

In the quiet corona, the radio radiation arises due to the thermal bremsstrahlung, the free-free emission. Over the intense magnetic fields of sunspots and active regions, gyroresonance emission plays role in the emission of radio waves. This radio emission from the Sun's surface is further discussed in the next sections.

2.1.2 Active Sun

The activity of the Sun in all the layers depends on the phase of the solar cycle.

The photosphere has sunspots and faculae with strong magnetic fields, both varying with time, magnitude and location. Over the solar cycle, the sunspots appear and disappear as a source of solar activity. Magnetic field lines from the sunspots emerge to the chromospheric layer to form magnetic active regions. Magnetic reconnection, particle acceleration and instabilities in these complex magnetic field in the chromospheric and coronal surfaces lead to the dynamic phenomena like flares, coronal mass ejections, and solar bursts.

During flares, radio emission is observed in the flaring active region, at the coronal layers of lower densities, and up to several solar radii from the Sun. Highly energetic electrons produced in the flaring region produce impulsive hard X-rays and the microwave radiations.

Aschwanden and Benz (1997) used synchrotron radiation from the relativistic electrons having energy of order a few MeV to locate the acceleration site in low corona. Imaging the locations of some of the impulsive radiation in the low corona over the active regions, and just above the top of coronal EUV and soft-X-ray loops, can be done using VLA measurements (Lang, 1998). At times outside of flares, it is recognized that

the radio detection of gyroresonance emission at microwave wavelengths could be used to determine the coronal magnetic field in the active region (Ginzburg and Zheleznyakov, 1961).

2.2 Radio Observations

Radio observations cover a broad frequency range from sub-millimeter to kilometer wavelengths, and sample different heights and physical conditions in the solar atmosphere. Radio emission and the propagation of radiation in the solar atmosphere leads to changes in the spectrum, which can be used to understand the atmospheric parameters along the line of sight of the observation.

The three relevant frequencies (Gary & Hurford, 1988) in the emission mechanisms are the plasma frequency,

$$\nu_p = 8.98 \times 10^3 \sqrt{n_e}, \tag{2.1}$$

The free-free emission frequency with unity optical depth,

$$\nu(\tau_{\rm ff} = 1) \approx 0.5 n_e T_e^{-3/4} L^{1/2}, \tag{2.2}$$

and the electron gyro frequency

$$\nu_B = 2.8 \times 10^6 B. \tag{2.3}$$

Here n_e is the electron density in cm^{-3}, T_e is the electron temperature in K, L is the scale length for free emission in cm, and B is the magnetic field strength in G.

The characteristics radio frequencies to height in the solar atmosphere of a nominal solar model is shown in Figure 2.3. The characteristic frequency that appears highest determines the emission mechanism of the radiation. The frequencies from 30 KHz to

few hundred MHz is dominated by plasma emission covering heights greater than 0.2 R_{sun} (Solar radius) above the photosphere because of τ_{ff}=1 level. At the decimetric frequencies, τ_{ff}=1 level with the plasma emission is important because of the inhomogeneity of the corona and the extremely high brightness of the coherent plasma emission reaching 10^{15} K.

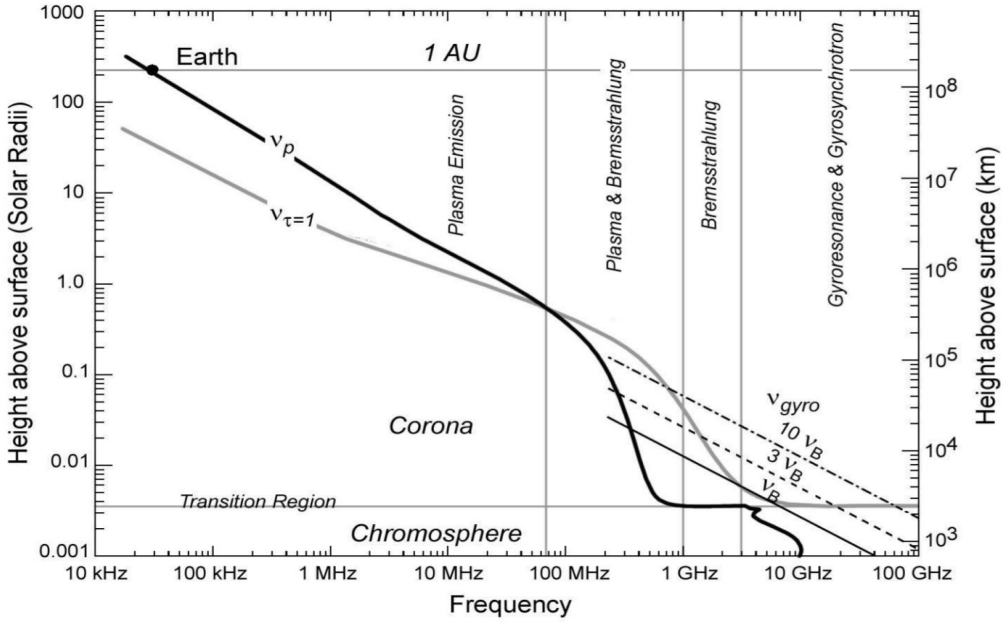

Figure 2.3 characteristics radio frequencies for the solar atmosphere (Gary & Hurford, 2004).

The cyclotron frequency and its harmonics are shown in three lines, where ν= 3 ν_B line lies above the τ_{ff}=1 level down to 1-2 GHz and extending to ~20 GHz. At ν=10 ν_B, gyroemission during bursts extend to 800-900 MHz in the decimetric range. Free-free gyroemission is dominated in mm wavelengths ~100GHz.

The incoherent emission mechanism of the radio radiation observation relevant to the current study can be described in two ways: Bremsstrahlung or free-free radiation and gyromagnetic radiation (Bastian, 2004).

2.2.1 Free-free Emission

The thermal free-free emission is due to the collisions between thermal electrons and ions on the Sun. This radiation can be used to diagnose quiet Sun, active regions, and flare decay phase.

2.2.2 Gyroresonance Radio Emission

Thermal gyroresonance emission is due to the gyrating motion of thermal electrons in the presence of magnetic field. This radiation is helpful in measuring the magnetic fields of active regions, where the magnetic field strength is high enough to make the corona optically thick to absorption in the frequency range of 1-18 GHz.

Thermal and non thermal gyrosynchrotron emission in the frequency range >1-2 GHz are generated by extremely hot electrons or a non thermal distribution of electrons. This radiation can be used to diagnose flaring sources.

In gyroresonant sources above the active regions $\nu_b > \nu_p$ ($n_e=10^{10}$ cm^{-3} and B>=300 G). There are two circularly polarized electromagnetic modes in such plasma conditions. Extraordinary or 'x' mode gyrates the magnetic field like an electron and resonates with the thermal electron population. The ordinary or 'o' mode is another mode that gyrates the magnetic field in the opposite direction to that of an electron.

2.2.3 Coronal Magnetic Field Measurement

The absolute value of coronal magnetic field strength is important to determine the energetics of the corona, free energy stored in magnetic fields which may be useful to understand flares and coronal heating.

The outer edges of the radio sources contain information on the magnetic field strength at the base of the corona. In each mode of radiation several harmonics can be identified required for determining absolute values of B (Gary & Hurford, 1994).

A physical model of an active region is proposed by Mok et al. 2004 extrapolated from an actual vector magnetogram. Assuming the volumetric heating rate is directly proportional to the local magnetic field strength, the thermal structure is computed (Gary & Hurford, 2004). The radio emission that would be observed is predicted with a given three dimensional model. The spectra with maps at 100 frequencies is shown in Figure 2.4.

In both the polarization spectra, the ratio between the sharp edges detected is 2:1, implying that they are first and second harmonics. Determining the harmonic number, the frequency of the edge is detected and the magnetic field at the base of the corona is determined.

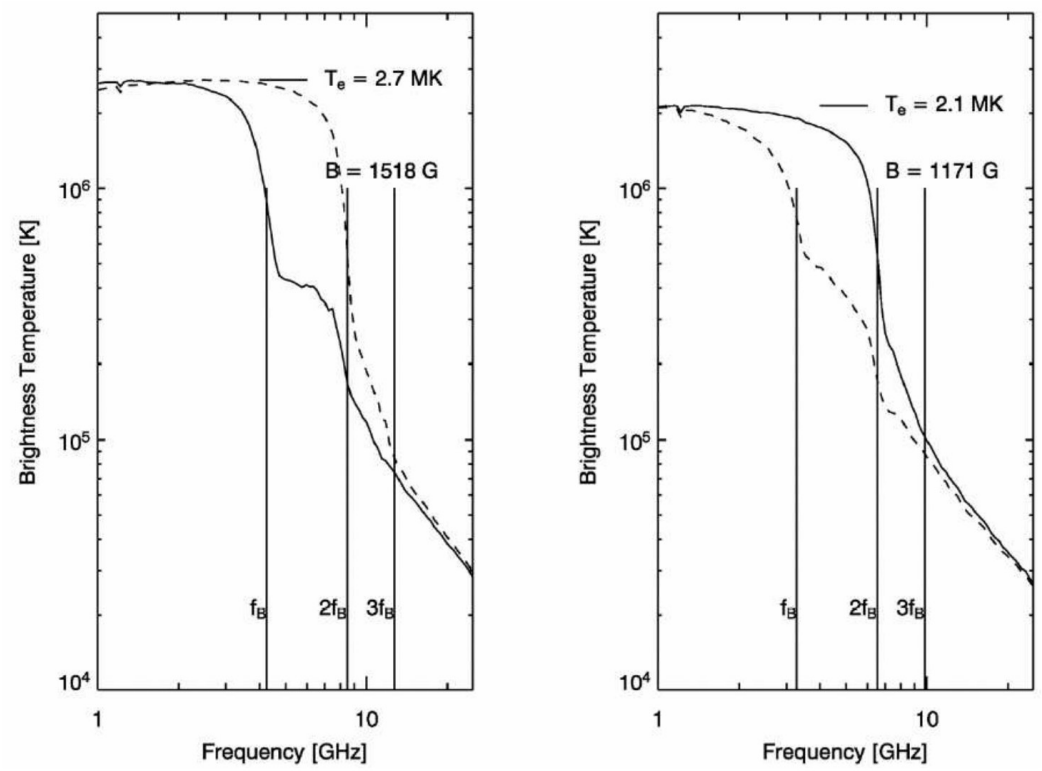

Figure 2.4 The right-hand (solid curve) and left-hand circular polarization radio emission spectra at two lines of sight in a model active region calculated at 100 frequencies from 1-24 GHz.

CHAPTER 3

DATA AND OBSERVATION

3.1 JVLA Interferometer

The Very Large Array, one of the world's premier astronomical radio interferometers, consists of 27 radio antennas in a Y-shaped configuration on the Plains of San Agustin fifty miles west of Socorro, New Mexico (latitude = 34.1, longitude = 107.6, elevation = 2124 m (6970 ft)). Each antenna is 25 meters (82 feet) in diameter. The data from the antennas is combined electronically to give the resolution of an antenna up to 36 km (22 miles) across, with the sensitivity of a dish 130 meters (422 feet) in diameter. The resolution of the VLA is set by the size of the array. At its highest frequency (43 GHz) this gives a resolution of 0.04 arcseconds (http://www.vla.nrao.edu/).

EVLA (Expanded VLA) is the major expansion of the VLA with the upgraded telescope, referred to as the Karl G. Jansky Very Large Array (JVLA). JVLA aims to have a full frequency coverage from 1 to 50 GHz (30 to 0.7 cm) with 8 frequency bands: L (1-2 GHz), S (2-4 GHz), C (4-8 GHz), X (8-12 GHz), Ku (12-18 GHz), K (18.0-26.5 GHz), Ka (26.5-40.0 GHz), and Q (40.0-50.0 GHz) providing improved observational capabilities over the original VLA.

Figure 3.1 VLA array in Y shape configuration.

Source: http://www.cv.nrao.edu/course/astr534/Interferometers2.html

The JVLA is a sensitive instrument which provides high spatial and temporal resolution to study the radio emission from the coronal loops and to study the radio bursts, but its longer baselines resolve out the relatively large-scale features of the Sun, making it most useful in its two smallest array configurations (C and D).

To observe the on-disk signatures of the Sun in this study, JVLA is used in the S-band, 2 to 4 GHz of observing frequency. On the day of eclipse, out of total 27 antennas 23 are used for the observation in both right and left polarization. The number of frequency channels is 16 in the range of 2 to 4 GHz. The array at the time of observations was in its (non-optimum) C and B configuration, in which the E and W arms were in the C configuration (3.6 km) and the N arm was in the more extended B configuration (10 km).

3.2 Observational Setup

The annular solar eclipse is observed from the JVLA interferometer on May 21 2012 in the early hours of the day starting from 00:34 UT to 00:57 UT. The path of the annularity of the eclipse is shown in the Figure 3.2 indicating the extent of the Sun obscured by the Moon when observed from the regions on the Earth's surface.

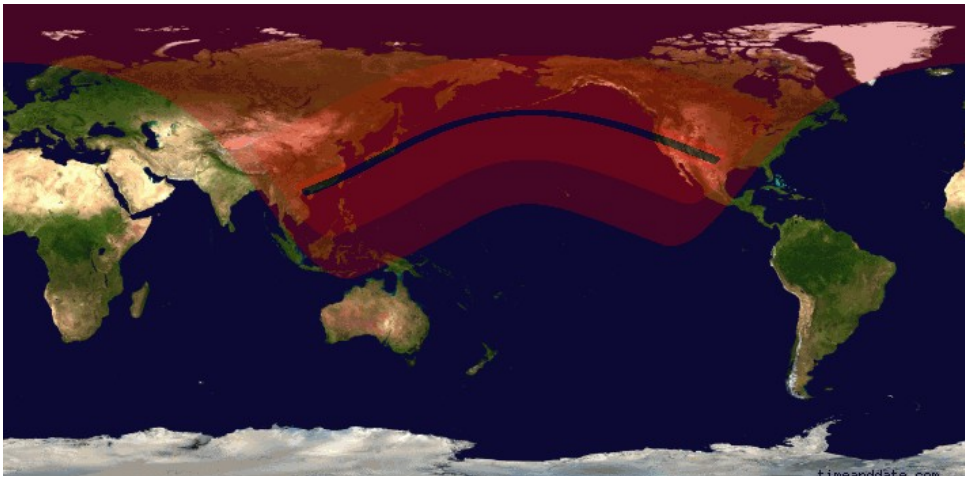

Figure 3.2 The path of annularity over the globe. The dark strip shows the locations from the Moon moves completely annular in the centre of the Sun, where JVLA site falls in. The shaded red shows locations with lesser part of solar disk obscured. The fainter red shows even less the Sun's disk obscured during the eclipse.

Source: http://www.timeanddate.com/eclipse

The study concentrates more on the on-disk observation after the first contact than the total annular observation of the Sun, because annularity occurred too late, when the Sun was already below the elevation limit of the antennas. On the solar disk, either an active region or quiet Sun region can be observed during the eclipse. The eclipse observation on an active region leads to image the spatially resolved magnetic structure of the active region. Before and after the occultation of the active region the quiet Sun region can be imaged.

On the day of the May 21, 2012 annular eclipse, in the field of view of JVLA, two active regions 11482 (N15W44) between 00:34-00:45 UT, 11484 (N10W17) between 00:51-00:57 UT are observed in the path of occultation. The 23 antennas in the array progressively track the regions on the Sun's surface occulted by the Moon's passage. The array response of complex visibility data is recorded in both right and left hand circular polarization at 13 channels in the frequency band of 2 to 4 GHz with integration time of 1, 5 and 10 s. The two active regions are named as AR1 and AR2 throughout this study.

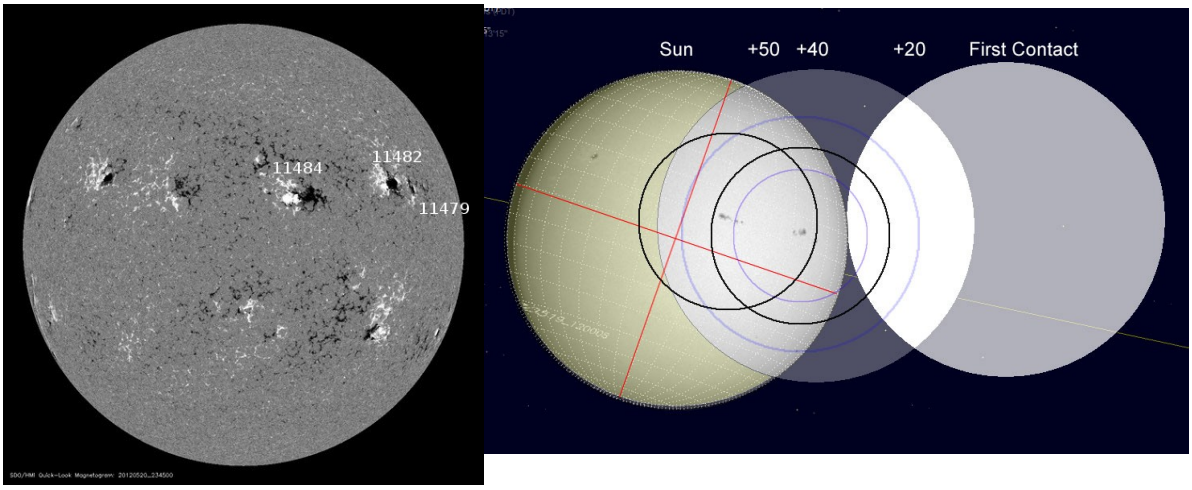

Figure 3.3 The uneclipsed Sun as seen in HMI magnetogram (left). The eclipse geometry (right) showing the Moon at first contact+40 minutes. The two regions are well occulted by the Moon as it passes through, which is shown in the dull shaded circle. The smaller black circles are the full width half power (FWHP) primary beam at 3 GHz and the two different-sized blue circles show the FWHP beams at 2 and 4 GHz correspondingly.

Source: http://sdo.gsfc.nasa.gov/data/aiahmi

Figure 3.3 (left) shows the HMI (Helioseismic and Magnetic Imager) magnetogram from SDO on orbit at 23:45 UT of May 20,2012. The active regions show a clear, simple bipolar structure. The geometry of the eclipse is pictured with the HMI intensitygram on May 19, 2012 at 12:00:08 UT and the first contact of the Moon is shown in the Figure 3.3. The corresponding full width half maximum (FWHM) primary

beam sizes of the observing frequency in 2 to 4 GHz range are marked in circles over the field of view.

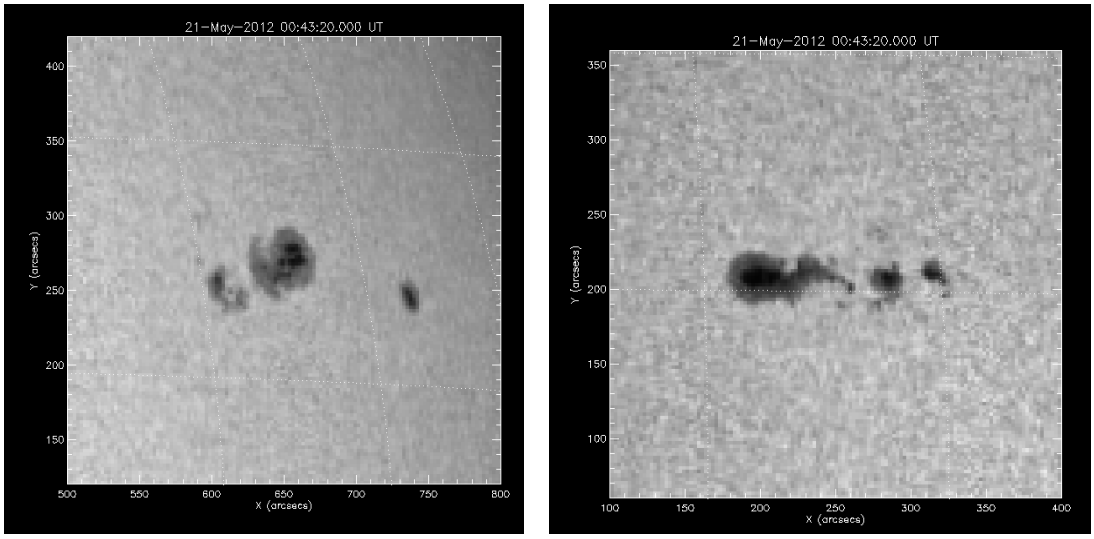

Figure 3.4 Close-ups of and AR 11482 (left panel) and AR 11484 (right panel). These are oriented with solar north up (i.e., no P angle). The x,y centres in arcsec W and N are 250, 210 (left panel) and 650, 270 (right panel). The AR 11479 is at 740, 240 arcsec in the right panel.

Source: http://sdo.gsfc.nasa.gov/data/aiahmi/

The close up images of the active regions AR1 and AR2 from the HMI images show the clear bipolar structure in Figure 3.4. AR 11479 (paired with AR1) is also occulted in the field of view, which does not have much role in the brightness distribution from the observation.

3.3 Data Structure and Tools Used

The two-dimensional complex visibility data from the eclipse observation is obtained in 1s, 5s and 10s of integration for the 13 frequency channels in all the baselines. The 10 s .fits (Flexible Image Transport System) and .uv visibility extension data files of the two active regions are studied separately. For analyzing these data sets of 'uv' visibility data, programming packages as shown below are used in different stages of the analysis.

AIPY-MIRIAD

AIPY (Astronomical Interferometry in Python) is a package which collects together tools for data from radio astronomical interferometry. Miriad is a Fortran interferometry data reduction package used for the reduction of continuum and spectral line observations from beginning to end, starting with the loading of the data through to image synthesis, analysis and display with publication quality graphics. Miriad supports calibration and analysis of polarimetric data, multi-frequency synthesis imaging, mosaicing, and specialized spectral line observations.

AIPY-MIRIAD includes interfaces to MIRIAD-PYTHON, in addition to pure-python phasing, calibration, imaging, and deconvolution code.

MIRIAD-PYTHON

The MIRIAD-python is a open-source software package that provides a bridge between the Python programming language and the MIRIAD package. It provides facilities for:

- reading and writing MIRIAD datasets in Python,
- executing MIRIAD tasks from Python, and

- implementing MIRIAD tasks in Python.

AIPY-MIRIAD is used to read the uv dataset which consist of two parts, variables and the data. Variables include the observing frequency, source name, (u,v) coordinates, baseline number and other parameters. Data is the actual intensity complex visibility from the interferometer.

IDL

IDL (Interactive Data Language) is a programming language used for data analysis in particular areas of science, such as astronomy and medical imaging. It has been widely applied in space science and in solar physics. It includes many advantages in working with image processing and in interactively processing large amounts of data.

CHAPTER 4

DATA ANALYSIS – MAPPING

The complex visibility calibrated data in 10 second integration of both the active regions are mapped, cleaned and analyzed individually in nominally the 16 frequency bands of 125 MHz each that cover the 2-4 GHz range. However, radio frequency interference (RFI) badly affected the calibration of bands 2, 3, and 4, leaving only 13 bands (1, and 5-16). The synthesis mapping technique for the analysis is employed with the same method used in previous eclipse studies. The difference between the visibilities in two successive integrations is due entirely to the emission from the narrow strip of the Sun that is covered or revealed by the Moon's motion during the integration. This technique has been demonstrated successfully several times (Gary et al. 1993, White & Kundu 1994, Marsh, Hurford, and Zirin 1980, Gary and Hurford 1987).

4.1 Calibration

Calibration of observations is not only important for tracking instrumental phase and gain drifts, atmospheric and ionospheric gain and phase variations, but for monitoring the quality and sensitivity of the data and for spotting the occasional gain and phase jumps (https://science.nrao.edu).

A sufficiently strong source is chosen as a calibrator closest to the source in observation. Atmospheric phase fluctuations are better calibrated if the calibrator in calibration is within 10 degrees.

Before observing the Sun for eclipse, calibration is done with a known calibrator source for 2 minutes observation. For the Sun and for calibration the bandwidth is 8 GHz. The phase calibrator used was J0555+3948, and the absolute flux calibrator was 3C48. The phase calibration is made more difficult because of the extremely low elevation of the Sun near the end of the observations. To obtain the longest possible time on the Sun, the dishes are tracked as low as 8 degrees of elevation, meaning that the signal path was traveling through a long path through the Earth's atmosphere, which leads to increased phase fluctuations, especially for the very long baselines with the antennas in the B-configuration N arm of the array.

4.2 Light Curves and Spectra

The 10 s averaged visibility amplitude and phase time series in a selected baseline at 2.56 GHz for both the active regions is shown below in the Figure 4.1. The amplitude oscillations and the phase variations are characteristic of a moving "knife edge" covering and uncovering the extended solar brightness distribution (Marsh et al 1981).

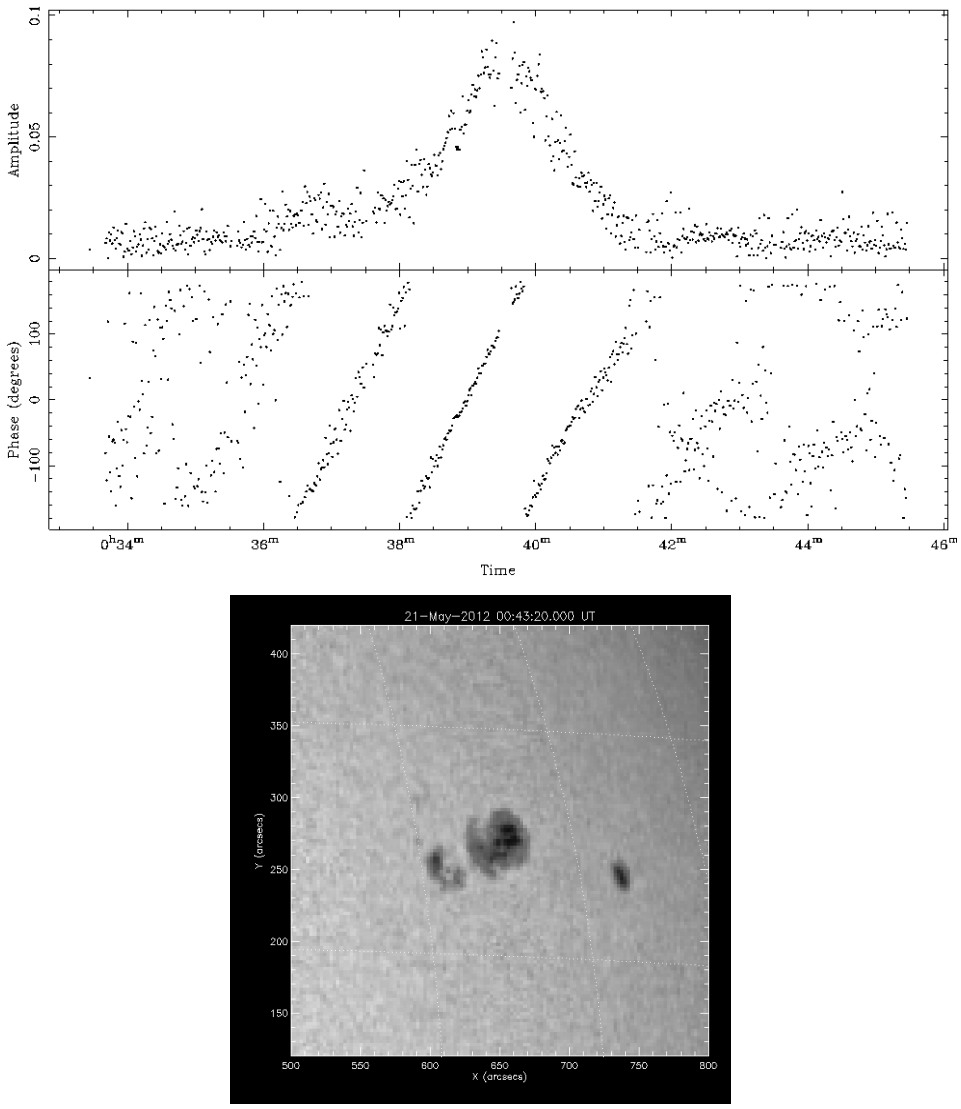

Figure 4.1 Peak brightness distribution in amplitude and phase variations of AR1 (upper panel) in right hand polarization at 2.56 GHz. The peak around 00:36:45 UT in the upper plot show the brightness enhancement due to the eclipsing of AR11479 which is covered earlier by the Moon as shown in map. Further AR1 is uncovered by the Moon which peaks around 00:39:40 UT.

As the Moon progresses over the Sun's surface, the amplitudes and phases of the two active regions are measured every shown in the Figure 4.1. With the sensitivity of the instrument, the peak amplitude for the AR1 shows ~90% increase over the quiet Sun region value before 00:36 UT and after 00:44 UT.

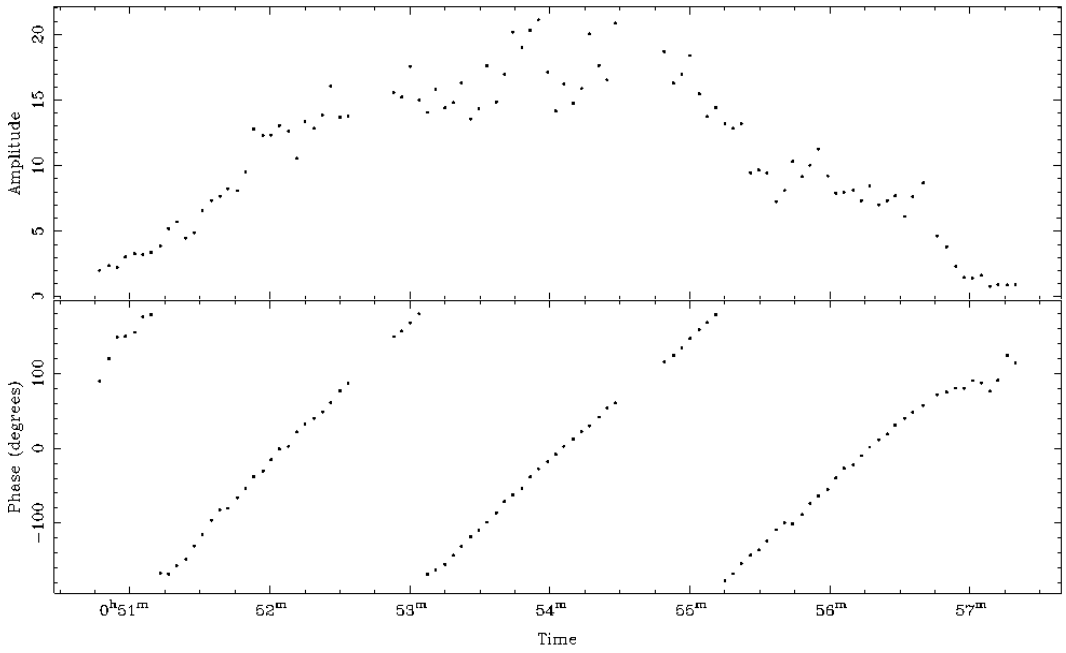

Figure 4.2 Time series of amplitude and phase variations of AR2 in right hand polarization at 2.56 GHz.

As seen in the amplitude plots in Figure 4.2, at the selected channel of frequency 2.56 GHz, the peak brightness temperature corresponding to second active regions also shows 90% increase over the quiet Sun region value (taken after 00:57 UT).

A spectrum is a brightness temperature distribution given by the Rayleigh-Jeans approximation for the Plank function

$$S_\nu = \int \frac{2k_B T_b \nu^2}{c^2} d\Omega, \tag{4.1}$$

where S_ν is the flux density (W m^{-2} Hz^{-1}) at frequency, ν (Hz), from the solid angle, dΩ, k_B is the Boltzmann constant and T_b is the brightness temperature.

A spectrum records the changing peaks in intensity as they evolve in frequency. Over the frequency band of 2 to 4 GHz, the brightness distribution dynamic spectra of AR1 as a function of time is shown in the Figure below. Few channels in the whole 16

channel band are blank as seen in the spectra. The peak intensity enhancement is observed at frequencies 3.3 and 3.4 GHz, which validates the results of the study of change in the emission mechanism by Gary and Hurford 1987. At these frequencies, the source region show a quick broadening and then continues with increasing frequency. The enhancement due to AR 11479 is consistent in almost all the frequencies at around 00:37:00UT. The features of parallel spikes are observed after 00:42:00 UT continue to the end, which may be real or artifacts.

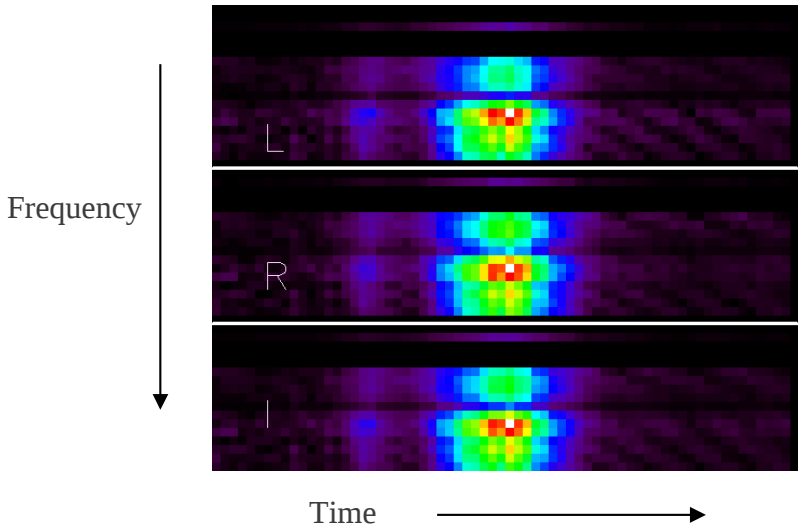

Figure 4.3 Dynamic spectrum of AR1 as a function of frequency (2 to 4 GHz) with time averaged over 10 s in left, right hand circular polarization and total intensity for a selected baseline.

4.3 Mapping

Initially, for mapping the visibility data, single frequency channel at 2.56 GHz is selected for the whole time range of 10 s integrated data of the eclipse observation. The running difference of each 10 s data represents the spatial features on the Sun's surface with the corresponding movement of the Moon. Because the window is moving across the active region, the flux variation with time represents the one-dimensional spatial variation (Gary and Hurford, 1987). The Figure 4.4 shows such a single differenced 10 s map overlaid with the positions of the Sun and the Moon limbs calculated from J2000 coordinates. The feature at -20,150 in the map tend to follow the Moon's limb over the time period. Even though it does not show much variations in its size, it shows intensity enhancement at the peak occultation than the regions where the Moon is away from the active region.

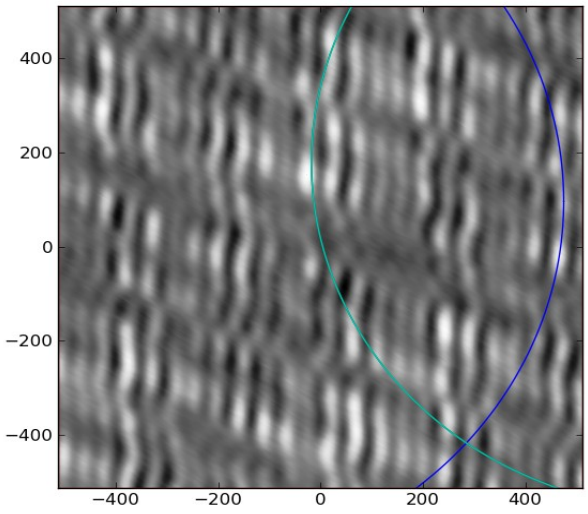

Figure 4.4 Uncleaned map with the Sun's (blue) and Moon's (green) limbs marked for AR2 at 2.56 GHz, 00:52:10 UT. As the Moon occults the Sun's surface, a feature at (-20,150) is seemed to follow the Moon's limb over time.

This difference map represents only the true information of a narrow annulus of 1.2 arcsec wide covered by the two consecutive positions of the Moon in 10 s. With the determined Moon's limb position, the restricted narrow annulus is extracted individually for every 10 s in the whole time duration of the Moon's passage over the active regions.

4.4 CLEAN Technique

Each annulus/strip of information is subjected to 'clean' with the parameters assuming the image to be an extended source. Clean Miriad task takes a dirty map and beam, and produces an output map which consists of the Clean components. This output can be input to 'Selfcal' routine to self-calibrate visibilities.

These cleaned maps of strips are merged one by one over time in a mosaic to generate a complete map of the active region (Gary and Hurford 1987) with intensity enhancements, if any. The resulting cleaned maps of both the active regions are shown in Figure 4.5 at 2.56 GHz in the whole period of Moon occulting the Sun's surface. The negative intensity pixels are constrained to non negative value in each clean map. However, a clear view of the active region is not extracted, but active region like feature at the centre of the map in AR1. The oscillatory structures in both the maps are due to the positive and negative side lobes of the synthesized beam.

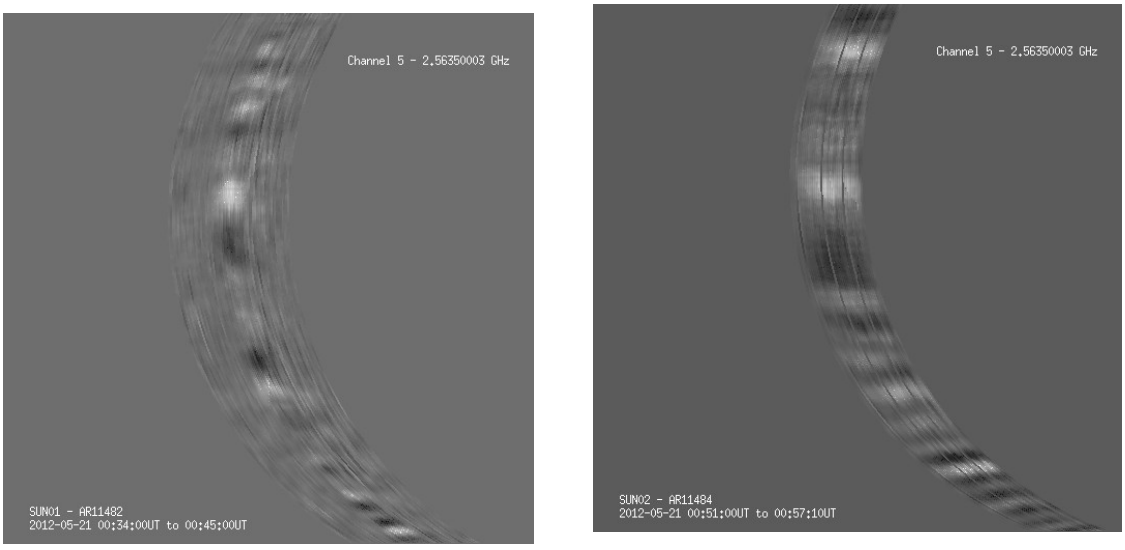

Figure 4.5 Cleaned maps merged over time give the orientation of the lunar limb to view the picture of the active regions AR1 (left) and AR2 (right) at 2.56 GHz.

The same procedure for clean imaging is used to view the complete occulted region by the Moon in all the 16 frequency bands in 2 to 4 GHz in right and left hand circular polarization. With the increase in the frequency, it is expected to see the change in the size and features of the active region for the brightness distribution at each frequency. When viewed with a movie clip of these frequency maps, the brightness emission moves continually downwards with frequency, which is not expected, if it is a fixed source like an active region. The same characteristics are observed for both the active regions.

4.5 Correlation with Space Borne Observation

The merged maps are overlaid on HMI magnetogram images at the peak differenced intensity (or at the Moon's limb over the intense activity part of the region). The overlay allows to correlate the actual position of the active region on the disk with the brightness distribution of the created cleaned radio map. The Figure 4.6 below shows the HMI

image when AR1 is at the peak magnitude of the eclipse at 00:38 UT. The clean map is at 3.3 GHz channel rotated by the position angle of -19.1 degrees.

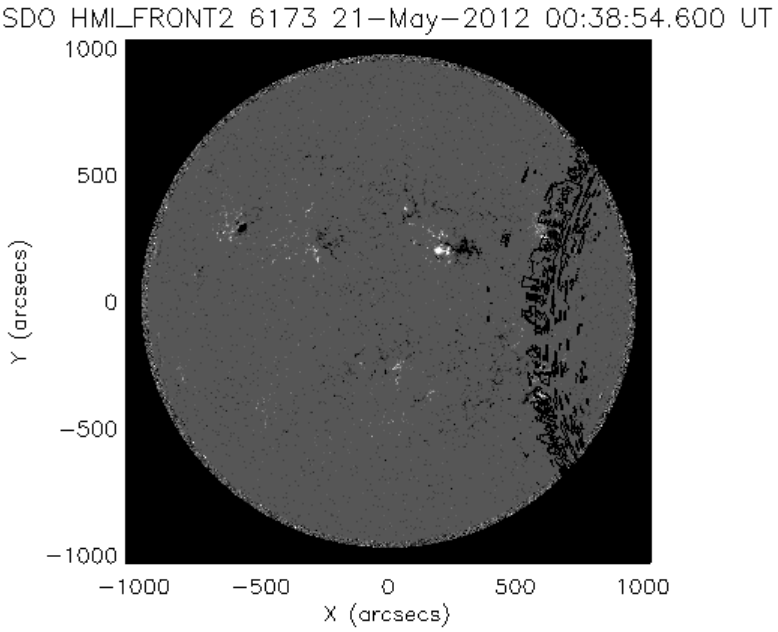

Figure 4.6 The JVLA eclipse clean map of AR1 at 3.3 GHz overlaid on HMI magnetogram. The bright source like feature seen in the clean map at (600,250) coincides with the active region 1.

The overlay maps show a good correlation between the orientation of the lunar limb in the clean map and the active region location in the HMI map. The overlay of AR2 clean map on the eclipse peak magnitude HMI map at 00:53 UT with position angle correction is shown in the Figure 4.7.

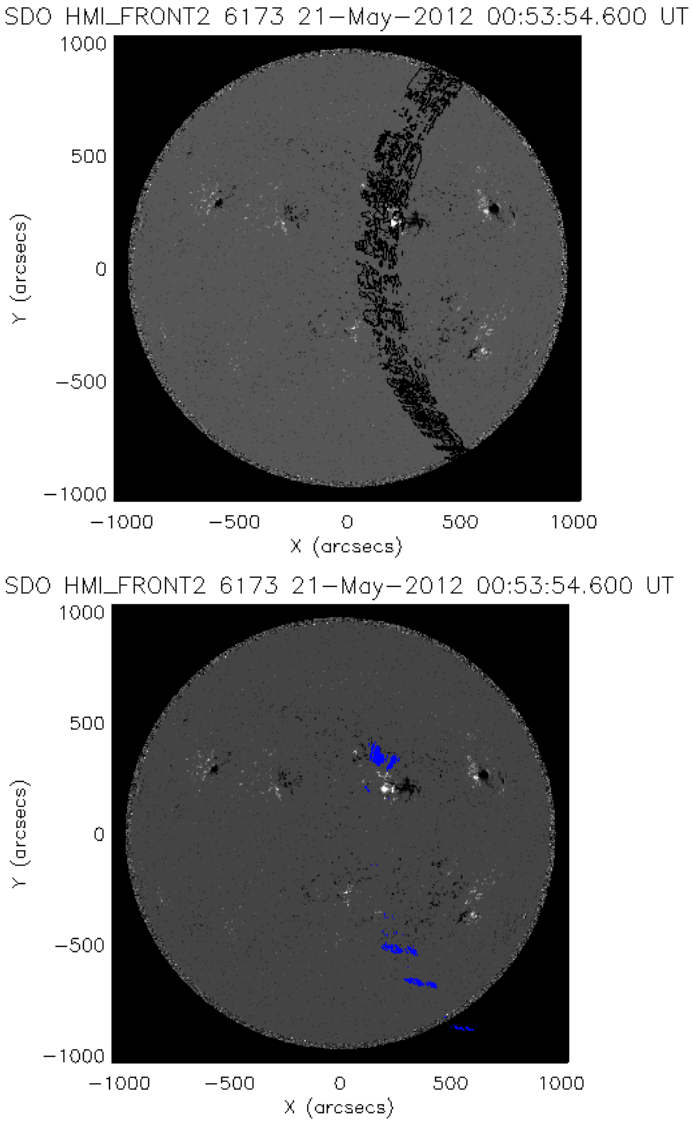

Figure 4.7 The JVLA clean map overlaid with the HMI magnetogram at 00:53, peak of the eclipse on AR2. The contour overlay of clean map at 90, 80, 70 and 60% seems to coincide with the active region location.

The contour map of the clean map coincides with the active region but with some error (which may be due to the position angle correction of the HMI map aligned with the clean map). The features seen at the lower right of the map are the side lobes of the main source.

CHAPTER 5

CONCLUSION

The Objective of annular eclipse observation is to provide high spatial resolution of the obscured regions on the Sun’s surface during the eclipse with radio measurements. The eclipse is observed in the solar minimum activity period of solar cycle 24, where no prominent flare events are reported. Hence, the observations allowed to study the structure of active regions and quiet Sun regions.

Rather than observing the Sun during the eclipse as a whole map of the entire field of view, differential technique is used to map strips of the field of view covered and obscured by the Moon's limb. This study is an attempt to understand the active region structures and the quiet Sun regions by realizing the change in the intensity levels of the observation than the intensity itself. At the selected frequency of 2.56 GHz, the peak brightness temperature corresponding to both the active regions show 90% increase over the quiet Sun region value.

Even though the bright source like feature in the synthesis map does not show much variations in its size, it shows intensity enhancement at the peak occultation than the regions (quiet Sun) where the Moon is away from the active region. As the synthesis mapping from the data does not produce very good high spatial maps of complex coronal structure, it is required to check with the calibration errors and improve the mapping as its further analysis. However, the HMI overlay with the radio map gives a reasonable correlation.

REFERENCES

Alissandrakis C. E., Kundu M. R., and Lantos P. 1980, Astron. Astrophys, 82, 30-40

Arvind Bhatnagar 2005, Fundamentals of Solar Astronomy, William Livingston, World Scientific Publishing Co. Pte. Ltd.

Aschwanden, Markus J., and Benz, Arnold O. 1997, Astrophys. J, 480, 825

Bastian, T. S. 2004, in Solar and Space Weather Radiophysics: Current Status and Future Developments, ed. D. E. Gary & C. U. Keller, 314, Springer, 47-69

Gary, Dale E., and Hurford, G. J. 1987, Astrophys. J, 317:522-533

–. 1988, Bulletin of the American Astronomical Society, 20, 713

–. 1994, Astrophys. J, 420, 903-912

–. 2004, in Solar and Space Weather Radiophysics: Current Status and Future Developments, ed. D. E. Gary & C. U. Keller, 314, Springer, 71-87

Gary, Dale E., Leblanc, Y., Dulk, G. A., and Golub, L. 1993, 412, 421-430

Ginzburg and Zheleznyakov, 1961, Soviet Astronomy, 5, 1

Lang K. R. 2009, The Sun from space, Second edition, Springer

Lang, K. R., and Willson, R. F. 1982, Advances in Space Research, 2, 91-100

Mok, Y., Lionello, R., Mikic, Z., & Linker, J. 2004,
American Geophysical Union, Fall Meeting 2004, abstract #SH13A-1159

Mark Littmann, Fred Espenak and Ken Willcox 2008, in Totality Eclipses of the Sun, Third edition, Oxford University Press Inc.

Marsh, K. A., Hurford, G. J., and Zirin, H. 1980, Astrophys. J, 236:1017-1025

–. 1981, Astron. Astrophys, 94, 67-71

Mason H.E., and Tripathi D. 2008, in Recent Advances in Solar Physics, Active Region Diagnostics, Physics of the Sun and its Atmosphere, Proceedings of the National Workshop (India), World Scientific Publishing Co. Pte. Ltd.

White, S. M. 2004, in Solar and Space Weather Radiophysics: Current Status and Future Developments, ed. D. E. Gary & C. U. Keller, 314, Springer, 89-114

White, S.M., & Kundu M. R. 1994, in IAU Symposium 154: Infrared Solar Physics, ed. D. M. Rabin, John, T. Jefferies, and Lindsey C., 167

Willson, Robert F., Lang, K. R., Thompson B., Scheuehle, U., and Zarro D. M. 1998, in Cool Stars, Stellar Systems and the Sun, ASP Conf. Ser. 154, The Tenth Cambridge Workshop, ed. R. A. Donahue and J. A. Bookbinder, 727

Willson, Robert F., and Groff, Tyler D. 2008, Solar Phys, 250: 89-105

http://web.njit.edu/~gary/728/Lecture6.html [cited 2013 July 28]

http://www.nrao.edu/index.php/about/facilities/vlaevla [cited 2013 July 29]

http://ircamera.as.arizona.edu/Astr_518/interferometry1.pdf [cited 2013 July 28]

https://science.nrao.edu/ [cited 2013 July 28]